A-type Stars, the Destroyers of Worlds: The Lives and Deaths of Jupiters in Evolving Stellar Binaries

Alexander P. Stephan[1,2] , Smadar Naoz[1,2] , and B. Scott Gaudi[3]

[1] Department of Physics and Astronomy, University of California, Los Angeles, Los Angeles, CA 90095, USA; alexpstephan@astro.ucla.edu
[2] Mani L. Bhaumik Institute for Theoretical Physics, University of California, Los Angeles, Los Angeles, CA 90095, USA
[3] Department of Astronomy, The Ohio State University, Columbus, OH 43210, USA

Abstract

Hot Jupiters (HJs), gas giant planets orbiting their host stars with periods on the order of days, commonly occur in the Galaxy, including relatively massive (1.6–2.4 $M_\odot$, i.e., A-type main-sequence stars) and evolved stars. The majority of A-type main-sequence stars have stellar binary companions, that can strongly affect the dynamical evolution of planets around either star. In this work, we investigate the effects of gravitational perturbations by a far away stellar companion on the orbital evolution of gas giant planets orbiting A-type stars, the so-called Eccentric Kozai–Lidov mechanism, including the effects of general relativity, post-main-sequence stellar evolution, and tides. We find that only 0.15% of A-type stars will host HJs during their main-sequence lifetimes. However, we also find a new class of planets, Temporary Hot Jupiters (THJs), that form during the post-main-sequence lifetime of about 3.7% of former A-type main-sequence stars. These THJs orbit on periods of tens to a hundred days and only exist for a few 100,000 years before they are engulfed, but they reach similar temperatures as "classical" HJs due to the increased stellar luminosities. THJs' spin–orbit angles will mostly be misaligned. THJ effects on the host stars' evolution could also be observable for longer than a few 100,000 years. Overall, we find that approximately 70% of all gas giant planets orbiting A-type stars will eventually be destroyed or engulfed by their star, about 25% during the main-sequence lifetime, about 45% during post-main-sequence evolution.

Key words: binaries: general – planets and satellites: dynamical evolution and stability – stars: evolution – stars: kinematics and dynamics

1. Introduction

Exoplanets have been observed around a variety of host stars, with different masses, at all stages of stellar evolution, including main-sequence, subgiant and red-giant branch stages (e.g., Charpinet et al. 2011; Johnson et al. 2011b; Gettel et al. 2012; Howard et al. 2012; Barnes et al. 2013; Nowak et al. 2013; Niedzielski et al. 2015, 2016; Reffert et al. 2015). However, for massive, evolved stars, there appears to be a deficit in short-period or high-eccentricity planets (e.g., Johnson et al. 2007, 2008, 2010a, 2010b; Sato et al. 2008, 2013; Bowler et al. 2010; Schlaufman & Winn 2013). Furthermore, high metal abundances in so-called "polluted" white dwarf (WD) atmospheres indicate the presence of the remnants of planetary systems around these stars; the processes by which this material was brought onto the WDs is an active topic of research (e.g., Farihi et al. 2009, 2010; Klein et al. 2010, 2011; Melis et al. 2011; Zuckerman et al. 2011; Xu et al. 2013, 2017; Stephan et al. 2017).

The architectures of these planetary systems have become the focus of a rich field of research, as it was recently shown that dynamical processes play an important role in planetary system formation and evolution. These processes include resonant interactions (e.g., Lithwick & Wu 2012; Batygin & Morbidelli 2013; Petrovich et al. 2013; Goldreich & Schlichting 2014), planet–planet scattering (e.g., Rasio & Ford 1996; Chatterjee et al. 2008; Nagasawa et al. 2008; Beaugé & Nesvorný 2012; Boley et al. 2012), and secular perturbations from a companion (either a star or a planet; e.g., Fabrycky et al. 2007; Wu et al. 2007; Naoz et al. 2011, 2012, 2013a) or

from multiple planets (e.g., Wu & Lithwick 2011; Denham et al. 2018).

A particularly interesting group of discovered exoplanets are the so-called "Hot Jupiters" (HJs), which are gas giants that orbit their host stars on very tight orbits with periods on the order of a few days. While this class of exoplanets seems ubiquitous in the galaxy, it is noticeably absent in our own solar system. Several models have been developed to explain the formation and existence of these HJs, including gravitational perturbations of the planets' original orbits to high eccentricities, followed by tidal dissipation and orbit circularization and shrinking (e.g., Fabrycky & Tremaine 2007; Naoz et al. 2011, 2012; Beaugé & Nesvorný 2012; Petrovich 2015; Frewen & Hansen 2016), as well as disk migration during giant planet formation (e.g., Armitage et al. 2002; Masset & Papaloizou 2003; Armitage 2007). The idea that outer companions have perturbed these planets and led to high-eccentricity migration is also supported by recent observational campaigns that have shown that most HJs have a far away companion, either a star or a planet (e.g., Knutson et al. 2014), though it remains unclear if most of these companions can trigger high-eccentricity migration (e.g., Ngo et al. 2016). For a three-body system consisting of star–planet–star to be long-term stable the inner two bodies, the main star and the gas giant, have to be on a much tighter orbit than the third, outer, object, leading to a hierarchical configuration.

In recent years, so-called "retired" A-type stars, which are observed as K-type giants, have been focused on by many studies in attempts to discover exoplanets (e.g., Johnson et al. 2007, 2008; Bowler et al. 2010; Johnson et al. 2010a, 2011a, 2011b). "Retired" A-type stars are stars that would be classified as A-type during their main-sequence

lifetimes, but that have evolved beyond the main sequence and are subgiant or giant K-type stars at their currently observed life stage. While main-sequence A-type stars usually rotate rapidly and have high surface temperatures, greatly impeding exoplanet detection through radial velocity measurements, "retired" A-type stars rotate slower, are cooler, and have allowed for the discovery of several exoplanets. Furthermore, several HJs have also been discovered around A-type main-sequence stars through exoplanet transits (e.g., Gaudi et al. 2017; Johnson et al. 2018).

The classification of "retired" A-type stars has been shown to be rather challenging, as different methods to determine stellar masses seem to yield different values (e.g., Lloyd 2011; Johnson et al. 2013; North et al. 2017; Stello et al. 2017; Ghezzi et al. 2018), implying that some of these stars might rather be "retired" F-type stars. There seems to be uncertainty over the validity of some methods when compared to precise astroseismological measurements. In this work, we avoid these classification problems by simply focusing on a particular range of stellar masses, between 1.6 and $3\,M_\odot$ (with masses above $\sim 2.4\,M_\odot$ technically belonging to the low-end B-type mass range). This intermediate stellar mass range broadly coincides with classical definitions of main-sequence A-type star masses (Adelman 2004), and we refer to this mass range when labeling a star as A-type. A further discussion concerning A-type star evolution is given in the Appendix.

Stars more massive than the Sun, like A-type stars, reach post-main-sequence evolution much faster than smaller stars, and the vast majority of them have stellar companions (e.g., Raghavan et al. 2010; Moe & Di Stefano 2017; Murphy et al. 2018). Indeed, several A-type stars with HJs have companion stars (e.g., Johnson et al. 2018; Siverd et al. 2018). This leads to an interesting interplay of dynamical and stellar evolution effects that needs to be considered for planets in such systems. On the one hand, a hierarchical star–planet–star configuration will lead to secular oscillations of the orbital parameters due to gravitational perturbations by the outer companion on the planet's orbit, often leading to extreme eccentricities, the so-called Eccentric Kozai–Lidov (EKL) mechanism (Kozai 1962; Lidov 1962; Naoz et al. 2016). On the other hand, post-main-sequence stellar evolution will lead to, for example, stronger tidal dissipation or engulfment of close-in planets due to stellar radial expansion, and expanded orbits due to stellar mass loss. In this work, we study the combined interplay of these dynamical and stellar effects for Jupiter-sized planets in stellar binaries with A-type star primaries. We find that short stellar evolution timescales, high prevalence of binary companions, and strong tides during post-main-sequence evolution result in the destruction of nearly 70% of Jupiters orbiting A-type stars, more than we would expect for lower mass single stars. We propose that observed planets around intermediate mass main- and post-main-sequence stars with stellar companions[4] are consistent with our predicted results.

2. Numerical Setup

We perform large Monte-Carlo simulations that follow the dynamical evolution of hierarchical three-body systems, consisting of a relatively tight *inner binary* pair of a star and a Jupiter-sized planet, which are orbited by another star on a

distant orbit as *outer binary*. We solve the hierarchical secular triple equations up to the octupole level of approximation (the so-called EKL mechanism, e.g., Naoz et al. 2016), including general relativity effects on both inner and outer orbits (e.g., Naoz et al. 2013b), static tides between the primary star and the planet (following Hut 1980 and Eggleton et al. 1998; see Naoz et al. 2016 for the complete set of equations). Tides for radiative stars are also estimated to be much weaker than for convective stars, so we use different tidal models for (radiative) main-sequence and (convective) red-giant stars (e.g., Zahn 1977); however, observations are uncertain about their distinctiveness (Collier Cameron & Jardine 2018). The tidal Love numbers for stars and gas giants are set to 0.014 and 0.25, respectively (Kiseleva et al. 1998), and we choose a viscous timescale of 1.5 years for both. We also include the effects of stellar evolution on masses, radii, and spins on the two stars, as derived from the stellar evolution code SSE by Hurley et al. (2000). Unlike G- and F-type main-sequence stars, which exhibit magnetic braking due to their convective envelopes, A-type main-sequence stars are nearly completely radiative and do not experience significant magnetic braking (van Saders & Pinsonneault 2013). Their spin rates therefore do not substantially slow down during their main-sequence evolution lifetime, however, magnetic braking can occur during the red-giant phase after a convective envelope has formed, additionally to the slowing of the spin due to stellar expansion. These factors are included in the calculations performed with SSE and we also switch between tidal models for radiative and convective stars based on SSE determinations of evolutionary phases. Overall, the main differences between A-type stars and smaller stars lie in the much more rapid stellar rotation rate and the weaker tidal dissipation for radiative stars, which weaken the importance of stellar tides during the main-sequence lifetime. During post-main-sequence evolution, however, the massively expanded stellar radii, together with the more convective nature of red giants, greatly increase the strength of stellar tidal dissipation, beyond the strength of tides for less massive post-main-sequence stars. The interplay between the EKL mechanism and stellar evolution has previously been shown to play an important role in shaping the underlying dynamics and outcome of these systems (e.g., Kratter & Perets 2012; Shappee & Thompson 2013; Michaely & Perets 2014; Frewen & Hansen 2016; Naoz et al. 2016; Stephan et al. 2016, 2017; Toonen et al. 2016).

The mass of the primary star, $m_{\star,1}$, is taken from a Salpeter distribution with $\alpha = 2.35$ (Salpeter 1955); however, the mass range is restricted between 1.6 and $3.0\,M_\odot$ in order to ensure that the planet host star is an A-type or, at most, a small B-type star during its main-sequence lifetime (Adelman 2004). The stellar initial radii and spins are calculated using SSE by Hurley et al. (2000). Each primary star is given one planet, whose mass (m_p), size, and spin are set equal to those of Jupiter. The mass of the outer companion star, $m_{\star,2}$, is determined by the binary mass ratio distribution taken from Duquennoy & Mayor (1991). The semimajor axis, a_1 of the *inner binary* of the A-type star and Jupiter-sized planet is chosen uniformly between 1 and 10 au, while the *outer binary* orbit's semimajor axis, a_2, is again taken from the distribution in Duquennoy & Mayor (1991) for the stellar companion. The inner orbit's eccentricity is initially set to a small value, $e_1 = 0.01$, as are the stellar and planetary spin–orbit angles, since we assume that the planet was formed in a gaseous disk, while the outer orbit's

---

[4] Planetary companions might have different results.

eccentricity, e_2 is chosen uniformly between 0 and 1. To ensure long-term stability, we reject systems where a_2 is greater than $\sim$10,000 au, as galactic tides will tend to separate such systems relatively quickly (Kaib et al. 2013), and we only consider hierarchical systems to ensure long-term stability, which requires:

$$\epsilon = \frac{a_1}{a_2} \frac{e_2}{1 - e_2^2} < 0.1, \qquad (1)$$

and $a_1/a_2 < 0.1$ (e.g., Naoz et al. 2016). The inclination, i between the inner and outer orbit's angular momenta is chosen isotropically in cosine.

In total, we simulate 4070 systems using these parameter conditions, 3000 of which have a primary star mass smaller than about 2.4 $M_\odot$ and therefore are safely classified as A-type stars during their main-sequence lifetimes. We calculate the dynamical evolution of these systems for 13 Gyr, or until a stopping condition is fulfilled. If a planet touches the surface of a star or crosses the Roche limit, we stop the integration. We define the Roche limit $R_{\mathrm{Roche},A}$ of a body of mass m_A and radius r_A with respect to an orbiting body of mass m_B as:

$$R_{\mathrm{Roche},A} = 1.66 \times r_A \left(\frac{m_A + m_B}{m_A} \right)^{1/3}. \qquad (2)$$

Note that this equation simplifies to $R_{\mathrm{Roche},A} = 1.66 \times r_A$ and $R_{\mathrm{Roche},B} = 1.66 \times r_B \left(\frac{m_A}{m_B} \right)^{1/3}$ if $m_A \gg m_B$, as in the case of a star with mass m_A being orbited by a much smaller planet of mass m_B. The disruption of planets is highly sensitive to the Roche limit and thus to the numerical pre-factor value, chosen here to be 1.66. Numerical simulations by Guillochon et al. (2011) and Liu et al. (2013) suggested a larger value, (i.e., 2.7) while Faber et al. (2005) simulations found $\sim$2.2. Thus, choosing here a fiducial value of 1.66 means that the number of engulfed planets represents a lower limit on the fraction of planets that can be engulfed during post-main-sequence radial stellar expansion. On the other hand, this value might lead us to overestimate the number of planets forming HJs during the main-sequence lifetime (see Petrovich 2015).

3. Results

3.1. Classification of Dynamical Evolution Outcomes

From our 4070 simulated systems, about 70% ended in the destruction of the Jupiter-like planet, while in only 30% of cases did the planet survive to the WD phase of its host star. We identify several distinct groups of orbital evolution behaviors and outcomes for Jupiters around A-type stars in stellar binaries. There are mainly four such groups (see Table 1 for percentages):

1. Classical Hot Jupiters (CHJs): These are HJs on orbits shorter than about 10 days, as one would expect from previous studies of high-eccentricity migration (e.g., Fabrycky & Tremaine 2007; Wu et al. 2007; Naoz et al. 2011, 2012; Petrovich 2015). These planets reach their short-period orbits during the host stars' main-sequence lifetime due to an interplay of EKL-caused high orbital eccentricities and tidal effects. They are ultimately engulfed and destroyed as the stars evolve and expand.

Table 1
Jupiter Evolution Outcome Percentages

Phase	CHJ	RL-cross	THJ	Survived up to t_{Hubble}
Total	1.5%	31%	37%	30%
MS	1.5%	23%	…	…
Post-MS	…	8%	37%	…
WD	…	0.3%	…	30%

Note. Listed are classical HJ (CHJ), RL-crossing Jupiter (RL-cross), temporary HJ (THJ), and surviving Jupiter (survived), up to Hubble time, outcomes as percentages of the whole population of simulated systems. The percentages are given for the whole evolution of the stars (total), and also split between main-sequence (MS), post-main-sequence (Post-MS), and white dwarf (WD) phases.

About 1.5% of our systems experience this outcome. We further discuss this group in Section 3.2.

2. Roche-limit crossers: These are those planets that reach extremely large eccentricities through the EKL mechanism and cross their host stars' Roche limits or graze the stars' surfaces. We assume that they are destroyed upon crossing the Roche limit and end the computation of their orbital evolution. The actual fate of these planets might be more complicated, and some might even survive for an extended time after crossing the Roche limit (e.g., Faber et al. 2005; Dosopoulou et al. 2017; MacLeod et al. 2018); however, for simplicity, we mark them all as "RL-cross" in Figure 1. Some of the possible effects are discussed in Section 4.4. About 31% of our systems lead to Roche-limit crossing, 23% of which occur during main-sequence and 8% occur during post-main-sequence evolution. Those that cross the stellar Roche-limit during post-main-sequence evolution simply do not undergo high enough eccentricity excitations or are on initial orbits too wide to have short periapsis distances during the stellar main-sequence lifetime.

3. "Temporary" Hot Jupiters (THJs): These are planets that did not reach high enough eccentricities during the main-sequence lifetime of their host stars to experience tidal circularization and orbital shrinking, but which do so as the stars leave the main sequence and become giant stars. Virtually all of them only classify as "hot" Jupiters (in terms of temperature) for a short part of their total lifetime. They get engulfed as their host stars continue to expand and as tides continue to drive them to the stellar surface; however, their orbits usually do not fully circularize before engulfment. The engulfment process may result in energetic disturbances on the host star and might serve as an observable (e.g., MacLeod et al. 2018; see also Section 4.4). We find that about 37% of our systems experience this outcome; however, about a fifth of these (7% of all systems) reach this outcome even though the EKL perturbations by their companion stars are negligible, as their initial orbits are relatively close to the star, at about 1–3 au. Further details about this group are discussed in Section 3.3.

4. Surviving Jupiters: These are planets that never significantly interact with their host stars and survive until the stars become WDs. For this population, the companion stars' EKL perturbations were too weak to cause large eccentricities, and the planets' orbits were too
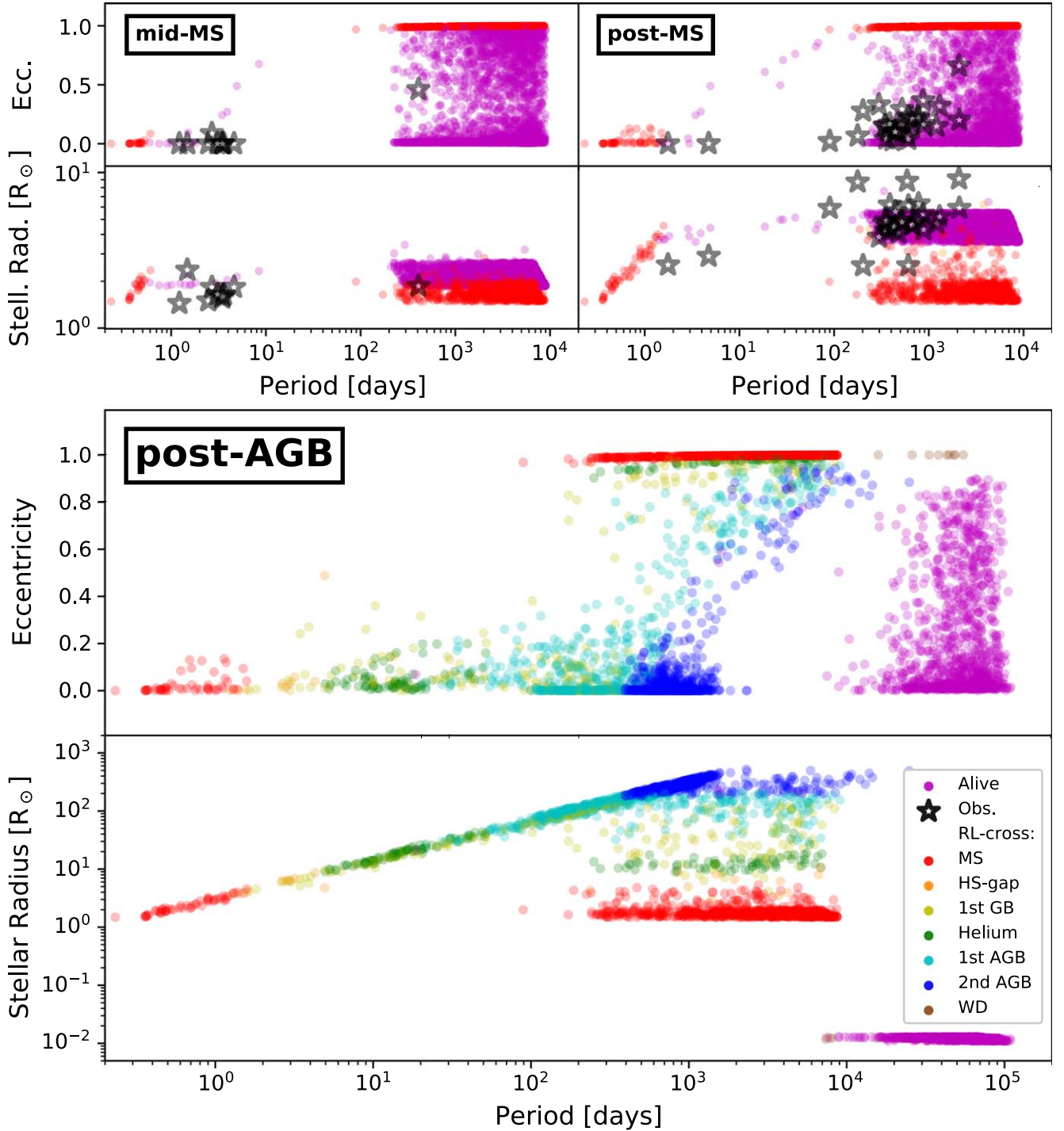
Figure 1. Dynamical evolution of Jupiters around A-type stars in binary systems. Top frame of each panel: Eccentricity vs. Orbital Period. Bottom frame of each panel: Stellar Radius vs. Orbital Period. The magenta dots show the parameters of Jupiters that survive to either the middle of the main-sequence (labeled mid-MS), the beginning of the post-main-sequence (labeled post-MS), or the white dwarf phase (labeled post-AGB). Differently colored dots show the final parameters for Jupiters that were destroyed by their stars either through EKL-induced high-eccentricity Roche-limit crossing or engulfment during stellar expansion. The colors represent the various stellar evolution phases at the time of planetary death: (red) main sequence, (orange) Hertzsprung gap, (yellow) first giant branch, (green) core helium burning, (cyan) first asymptotic giant branch, (blue) second asymptotic giant branch, and (brown) white dwarf phase. Out of 4070 planets, about 2870 were destroyed before 13 Gyr had passed, falling into two distinct main groups—(1) high-eccentricity, KL-driven deaths, and (2) low eccentricity, tidally, and stellar expansion driven deaths. The black stars are showing the positions of some observed Jupiters around A-type stars in this parameter space, see Section 3.2 for references.

wide to experience strong tidal effects during post-main-sequence evolution. This population mostly reflects our lack of knowledge on the initial conditions of these systems. About 30% of Jupiters survive to this stage. A small fraction of these (0.3% of all systems) gets

destroyed and accretes onto the WDs as the stellar mass loss changes the orbital parameters of the systems, allowing extreme excitations of the orbital eccentricities through the EKL mechanism, ultimately driving these Jupiters to cross their own Roche limits and to get tidally

disrupted by the WDs. Examples of this potential WD pollution mechanism have been discussed in detail in Stephan et al. (2017). Recent work (van Lieshout et al. 2018) also indicates that some of the planet's material can be recycled into new planets and escape accretion.

In Figure 1, we show three snapshots of the different systems' realizations during the stars' lifetimes, mid-main-sequence (top left), at the beginning of post-main-sequence (top right), and post ABG phase (bottom). We consider the eccentricity as a function of the planet's period (top panels). For comparison, we also plot the observed systems (depicted as black stars) for the relevant snapshot. For context, we also show the stellar radii for all of our systems (bottom panels). When a planet crossed the Roche-limit, we stop the integration and mark its orbital parameters.

Note the slight offset between the distribution of red and magenta points on the right side of the lower frame of the mid-main-sequence panel. This offset is simply caused by the red points showing planets that have been destroyed via EKL-driven high-eccentricity Roche-lobe crossing. This happens quickly, before the host stars can significantly evolve and expand. All the planets that lie in the region of the parameter space that allow such large eccentricities to be reached do so and get tidally destroyed or engulfed early in the systems' lifetime. By the middle of the main-sequence lifetime of the star, the rest of the systems have evolved more and their stars have expanded; however, there simply are not many planets left in the correct parameter space to cross the new, expanded Roche limit; they have all already been destroyed. However, once the stars swell to become red giants, there is a new phase of destruction of planets that did not reach extreme eccentricities. The difference in behavior between these two different populations is due to the distinction between "quadrupole" and "octupole" types of EKL evolution (see Naoz et al. 2016, for a full review of the EKL mechanism). Thus, we predict an early "burst" of planet destruction during the early main-sequence evolution, followed by a pause until the stars become red giants, followed by another phase of planet destruction throughout post-main-sequence evolution.

3.2. CHJs and Surviving Jupiters

As we show in Figure 1 (see upper panels), by the middle of the main-sequence lifetime of the host stars, several classical HJs have been formed through high-eccentricity migration (shown in the upper left panels as purple dots, with periods shorter than about 10 days and eccentricities close to 0), or are still in the process of forming until the end of the main sequence. However, these more massive stars expand their radius during the main sequence by about a factor of two, which results in a higher rate of Roche-limit crossing than for less massive stars, since the more massive stars evolve and expand more quickly and the Roche-limit is proportional to the radius of the star (see Equation (2)). In total, we form 64 such HJs, or about 1.5% of our systems, which is broadly consistent with, though somewhat less efficient than, previous estimates of EKL-induced high-eccentricity migration models in stellar binaries, which considered smaller mass host stars (see, for example, Naoz et al. 2012, 2016; Petrovich 2015; Anderson et al. 2016). Some of these classical HJs only survive for short times at these orbits, as the interplay of the EKL mechanism

and tides keeps driving them toward the stellar surface. However, many can exist for tens to hundreds of megayears after formation. Ultimately, though, all classical HJs get engulfed and destroyed as their host stars evolve and expand in radius. By the end of the main sequence, most of them have been destroyed (see the upper right panels of Figure 1; red dots show destroyed planets, with several red dots forming a line in the stellar radius versus orbital period parameter space where HJs were engulfed by their expanding host stars), with the remaining ones being destroyed as the stars evolve toward the giant phase (see the orange and yellow dots in the lower, large panels). In general, classical HJs around A-type main-sequence stars form at a lower frequency than HJs around smaller mass stars through high-eccentricity migration, and exist for shorter times due to faster stellar evolution, expansion, and tides.

The black stars in Figure 1 show the parameters of several observed Jupiters around A-type or retired A-type stars (Johnson et al. 2007, 2008, 2010a, 2010b, 2011a, 2011b, 2014, 2018; Collier Cameron et al. 2010; Sato et al. 2013; Bieryla et al. 2014; Wittenmyer et al. 2014, 2015a, 2015b; Hartman et al. 2015; Zhou et al. 2016; Beatty et al. 2017; Borgniet et al. 2017; Gaudi et al. 2017; Lund et al. 2017; Siverd et al. 2018; Talens et al. 2018), and they appear to be broadly consistent with our calculations. The observed HJs agree well with our predicted parameters at some time during the middle of the main-sequence lifetime of A-type stars (upper left panels), while observed Jupiters on wider orbits (periods beyond about 100 days) around retired A-type stars agree well with our predicted parameters for Jupiters that survive to the end of the main-sequence lifetime (upper right panels). Note that both observations and our predictions do not seem to show many Jupiters on intermediate orbits between 10 and 100 days. HJs migrate relatively fast through this part of the parameter space, on the order of a few million years (a very small fraction of the stars' total main-sequence lifetime), and are unlikely to be randomly observable.

3.3. Temporary Hot Jupiters

During post-main-sequence evolution, stars begin to expand, and those planets that have short pericenter distances are engulfed by their host stars. Furthermore, our calculations show that a large number of moderately eccentric giant planets will undergo significant tidal interactions with the expanding red-giant stars, leading to orbital shrinking and circularization before the eventual crossing of the Roche lobe or engulfment by the star, as shown by the example system evolution in Figure 2. During the red-giant phase, the strength of tidal effects on the star increases significantly due to the stellar radial expansion and the increased size of the convective envelope. During their main-sequence lifetime, A-type stars are mostly radiative, which severely reduces the effectiveness of their tides (Zahn 1977). We consequently observe a switch in the role of tides between the main-sequence and post-main-sequence evolution; while during the main sequence, the tidal effects on the planet were more significant, during post-main-sequence evolution, the tides on the star dominate. Tidal interactions and planet engulfment can be expected to have significant effects on the red-giant stars' envelope and mass-loss evolution, as well as changing the stellar rotation rate; such giant planet interactions with evolved stars have been used to explain observed irregularities in the shape of the horizontal branch in
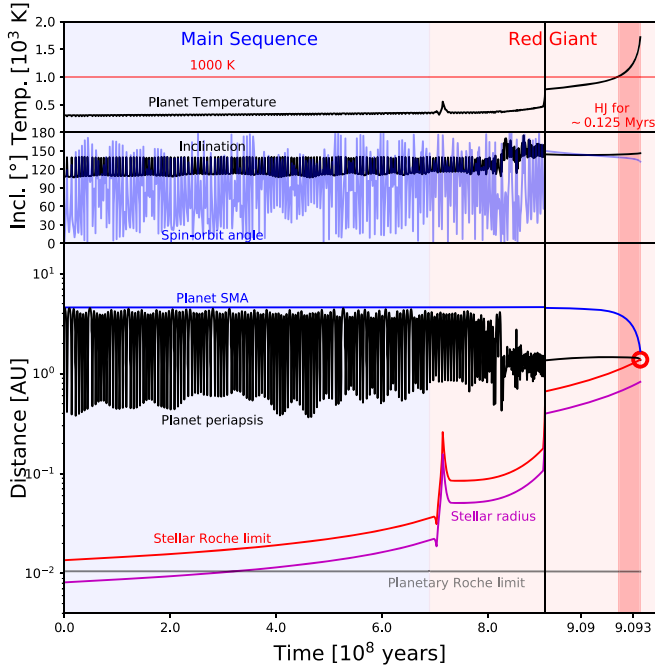
Figure 2. Orbital evolution of a Jupiter around an evolving A-type star in a stellar binary, leading to formation and destruction of a temporary hot Jupiter. The figure shows an example of Jupiter's equilibrium temperature (top frames), inclination, and spin–orbit angle (middle frames) and semimajor axis, periapsis, and stellar radius evolution (bottom frames) over time. In the bottom frames, the blue line shows the planet's semimajor axis, red and magenta show the host star's Roche limit and radius, and gray shows the planet's Roche limit. The blue shaded region marks the host star's main-sequence phase, while the red shaded area marks the post-main-sequence phase. The left frames of the figure show the first 908.8 Myr of evolution, while the right frames focus on the last 0.5 Myr before the planet enters the star's Roche lobe. Note that the planet's semimajor axis undergoes rapid tidal decay once the red-giant star has expanded sufficiently, on the very right edge of the figure. This rapid orbital decay lasts on the order of 300,000 years before the planet reaches the stellar Roche limit. The equilibrium temperature of the planet rises above 1000 K (marked by the red line in the top frames) for the last 125,000 years before entering the Roche lobe, rapidly increasing as the orbit decays, as highlighted by the darker red shaded area. Initial system parameters are $m_{*,1} = 2.39\ M_{\odot}$, $m_{*,2} = 1.95\ M_{\odot}$, $a_1 = 4.58$ au, $a_2 = 601.6$ au, $e_1 = 0.01$, $e_2 = 0.587$, spin–orbit angle $= 0°$, and $i = 108°.2$.

the Hertzsprung–Russel diagram (e.g., Soker 1998; Soker & Harpaz 2000; Livio & Soker 2002). Our "Temporary" HJs would most likely lead to such interactions, though we stop our calculations at the entering of the stellar Roche lobe. Further investigation would require a full hydro-dynamical treatment of the star–planet interactions. We assume that the further evolution of the stellar envelope and post-AGB remnant will be altered due to these interactions. THJ engulfment could also lead to lithium enrichment in the giant stars' atmospheres (e.g., Aguilera-Gómez et al. 2016).

The lower large panels in Figure 1 show the final orbital parameters of our systems in eccentricity versus period (upper frame) and host-star radius versus period space (lower frame). Those dots colored red, yellow, green, cyan, and blue show the final parameters before planets enter the stellar Roche lobe during the different post-main-sequence and pre-WD phases. The vast majority of these, those that form a distinct line on the left in the stellar radius versus period frame, experience at least some degree of high-eccentricity migration, and reach equilibrium temperatures comparable to classical HJs (see Figure 3). These planets begin to experience significant tidal interactions with their host stars as those stars expand in radius,

facilitated by increasing orbital eccentricities due to the EKL mechanism. However, due to the continued stellar evolution of the host stars and the significantly enhanced tides, most of these THJs enter their host stars' Roche lobe even before they can be fully circularized, making their status as HJs very short-lived. We therefore name this class of HJs THJs. The THJ shown in Figure 2 only lives for about 300,000 years once tidal orbital decay becomes efficient before it reaches the stellar Roche limit. This process should, as mentioned above, have significant effects on the further evolution of the giant star's outer envelope.

While most (∼80%) of the THJs we discuss here are products of high-eccentricity migration caused by the EKL mechanism and tidal dissipation and therefore depend on the presence of a companion star, some THJs can also be formed without a companion. If a gas giant's initial orbit is sufficiently close, in general, smaller than about 3 au, post-main-sequence expansion of the host star will eventually lead to tidal interactions and engulfment of the planet even without increased orbital eccentricity, consistent with previous works investigating the evolution of gas giants around giant stars (e.g., Villaver & Livio 2009; Spiegel & Madhusudhan 2012; Lopez & Fortney 2016). However, one can distinguish between these two cases considering the spin–orbit alignment of the planet and the main star. If a THJ is formed without companion excitations, the orbital plane will not change from its initial orientation, which we assume to be aligned with the stellar spin. If the THJ was formed through the EKL mechanism, however, the spin–orbit angle will be from a nearly uniformly random distribution between 0° and 180°. We can see this in Figure 4. The two histograms on the right side of the figure show the distribution of spin–orbit angles among THJs. Both histograms show the same population, only that the far right one labeled "THJs (all)" includes THJs formed both with and without EKL effects, while the one labeled "THJs (EKL)" only shows those formed through EKL effects. Those THJs formed without EKL effects, for which the stellar companion was irrelevant, are all aligned and form the large peak at 0°, while those formed with EKL effects are nearly evenly spread across the whole range of angles between 0° and 180°. While the peak is large, it is extremely narrow and only includes ∼20% of our total number of THJs.

4. Observational Signatures

4.1. Equilibrium Temperature

The equilibrium temperature of planets is a potentially observable signature (e.g., Gaudi et al. 2017). We calculate the time-averaged equilibrium temperature for elliptical orbits for the planets in our simulations, following equations by Méndez & Rivera-Valentín (2017), namely:

$$\langle T_{\mathrm{eq}} \rangle \approx T_0 \left[\frac{(1-A)L}{\beta \epsilon\, a^2} \right]^{\frac{1}{4}} \left[1 - \frac{1}{16}e^2 - \frac{15}{1024}e^4 + \mathcal{O}(e^6) \right],$$

$$(3)$$

where $T_0 = 278.5$ K, Earth's equilibrium temperature, A is the planetary albedo (assumed to be zero), L is the host star's luminosity (in $L_{\odot}$), e and a are the planet orbit's eccentricity and semimajor axis (in au), respectively, and β and ϵ are coefficients for the planet's heat distribution and emissivity, respectively (both assumed to be ∼1 for simplicity).
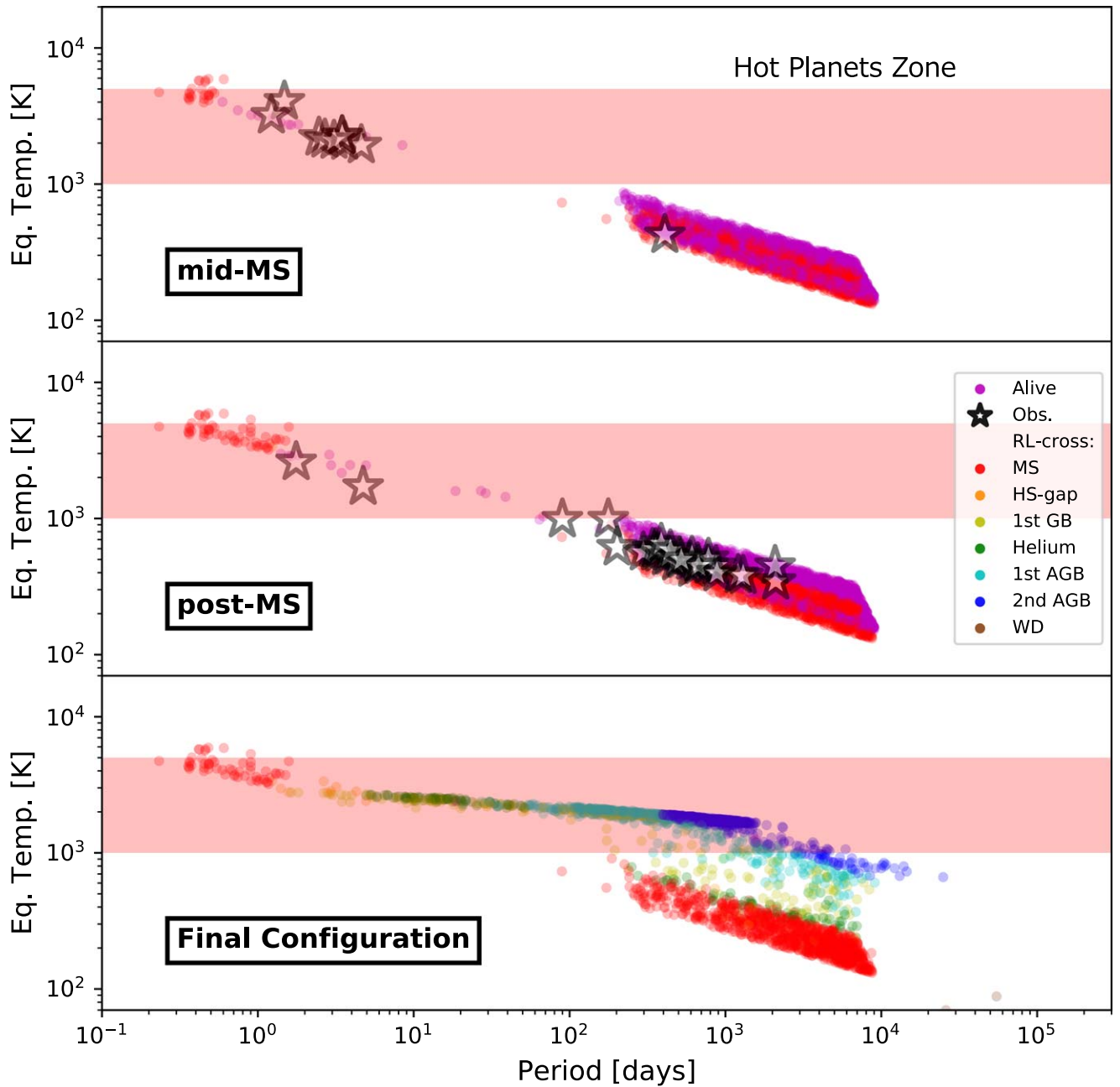
Figure 3. Equilibrium temperatures of Jupiters around A-type stars in binary systems. Equilibrium temperature vs. period of Jupiters for three evolutionary periods: middle of the main sequence (upper panel), beginning of the post-main-sequence (center panel), and the WD phase (bottom panel). Values for observed Jupiters around A-type stars are included as black stars. Dot colors have the same meaning as in Figure 1. The red shaded area shows the approximate parameter space of "hot" planet temperatures, from around 1000 to 5000 K. Note that THJs, which are within the red shaded area in the lower panel, can reach final equilibrium temperatures of several thousand Kelvin shortly before being destroyed, due to the intense stellar luminosity of the post-main-sequence host stars. Equilibrium temperatures were calculated using Equation (3) (Méndez & Rivera-Valentín 2017) for eccentric orbits, assuming zero albedo, or taken from papers cited in Section 3.2 for observed planets.

The classical hot Jupiters (CHJs) in our calculations have typical temperatures of about 2000–5000 K, consistent with estimated temperatures of observed HJs, as can be seen in the top frame of Figure 3, which shows our CHJs as magenta dots and observed HJs as black stars in the "Hot Planets Zone." CHJs remain at these temperatures for potentially millions of years, until they either evaporate or are engulfed by the host star as it leaves the main sequence (see the red dots in the middle frame of Figure 3. We find that THJs reach temperatures between 1000 and 3000 K just before entering the stellar Roche lobe, as shown in the bottom frame of

Figure 3. The THJs only exist at such high temperatures for a short time, on the order of a few 100,000 years, as seen in the top right frame of Figure 2, as the increase in temperature follows from the planets' rapid orbital decay and the rapid increase in stellar luminosity due to post-main-sequence stellar evolution. Considering that the stellar luminosity increases tremendously during post-main-sequence stellar evolution, even THJs will produce a rather small contribution to the overall stellar spectra. At a wavelength of around 1 μm, the contrast between THJ and stellar emissions will be around 10^{-5}–10^{-7}. Additionally, the expanding stars' large size will
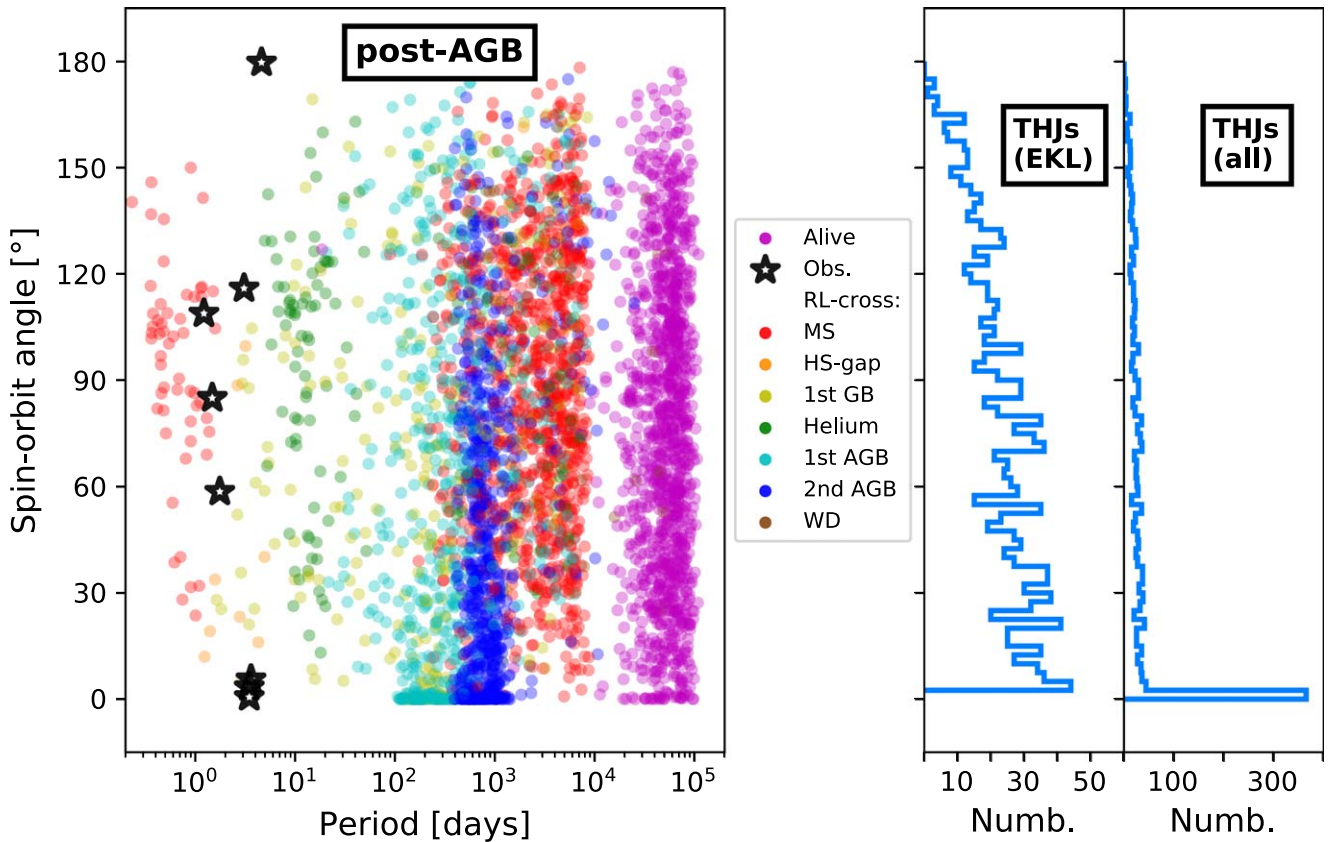
Figure 4. Spin–orbit misalignment angles for Jupiters around A-type stars in binary systems. Left large panel: Spin–orbit misalignment angle vs. period for Jupiters during the WD phase, with magenta dots showing survived Jupiters and differently colored dots showing destroyed Jupiters. Dot colors have the same meaning as in Figure 1. The plot shows that HJs, both classical and temporary, that form due to the EKL mechanism are most likely to have significantly misaligned orbits compared to their host stars' spin axes. This is broadly consistent with the few measured projected spin–orbit angles for HJs around A-type stars, shown by the black stars. THJs that form without the influence of the EKL mechanism are, in contrast, very well aligned (depicted by the blue and cyan points that are clustered near 0°). The two histograms in the right side panels show the distribution of misalignment angles for THJs. The far right histogram, labeled "THJs (all)," shows the spin–orbit angle distribution of all THJs, including both those formed with and without EKL effects, while the histogram to the left of it, labeled "THJs (EKL)," only shows those formed through EKL effects. Both histograms are practically identical except for the scale of the x-axis, which represents the number of simulated systems. The large peak at 0° inclination in the far right panel simply includes all non-EKL THJs. About 20% of THJs are in this peak and form without EKL effects, while about 80% of our THJs form through the EKL mechanism, spread across the rest of the spin–orbit angle parameter space.

make planet transit detection signals smaller as well; however, the larger size will also increase the chance that a transit can occur. At least for THJs around "small" giant stars ($R_* \sim 5\,R_\odot$), such as for stars during the helium burning phase, models suggest that transits are indeed observable (e.g., Assef et al. 2009), and some giant planets transiting giant stars of such sizes have indeed been observed (e.g., Lillo-Box et al. 2014), though it remains unclear if such transits would currently be observable for stars with sizes of hundreds of solar radii. However, if the increase in temperature leads to significant planetary inflation and if stellar high energy radiation or winds can drive a significant mass loss from the Jupiter, absorption lines from the stripped planetary material might be observable (e.g., Murray-Clay et al. 2009).

4.2. Stellar Obliquity

Detecting planets through the transit method makes it possible to observe the (projected) angle between the stellar spin axes and the planets' orbital planes through the Rossiter–McLaughlin effect (Gaudi & Winn 2007). Our calculations show that THJs, like CHJs, should preferentially be misaligned to the stellar spin axis, with a nearly uniform distribution of spin–orbit angles, showing only a small preference against

fully retrograde orbits, as can be seen from the THJ spin–orbit angle histograms in Figure 4. Using the spin–orbit angle, it should also be possible to distinguish THJs born through EKL effects from THJs without that effect, as the later will remain aligned to their original spin–orbit angle, which can be assumed to be small, close to 0° in our case. As can also be seen from the left frame of Figure 4, observed projected spin–orbit angles for HJs also broadly confirm a broad range of misalignment angles, potentially caused by EKL effects.

4.3. Orbital Eccentricity

The eccentricities of planetary orbits is an important factor for understanding the architectures of planetary systems, as larger eccentricities can be indicators of significant dynamical interactions, such as planet–planet scattering events or secular perturbations, while small eccentricity values are expected from disk models of planetary formation and a subsequently quiescent dynamical history. Massive evolved stars show a deficiency of short-period eccentric planets (Johnson et al. 2007, 2008, 2010a, 2010b, 2013; Sato et al. 2008; Bowler et al. 2010; Schlaufman & Winn 2013). Our calculations show that this feature is in agreement with the dynamical evolution of giant planets in stellar binaries. As
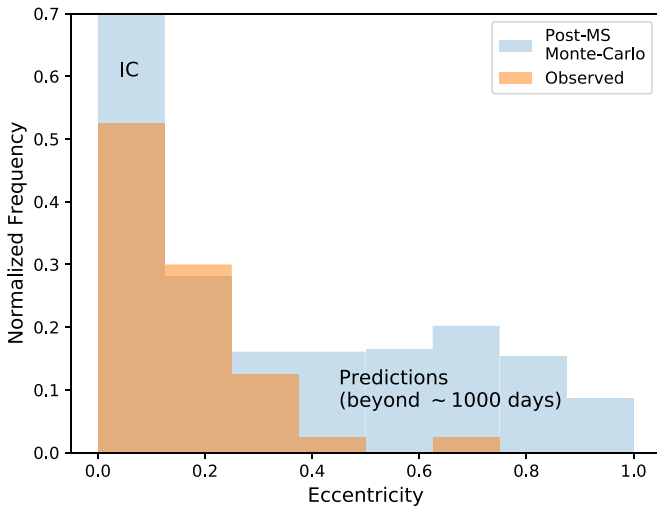
Figure 5. Simulated vs. observed eccentricity distributions for Jupiters around retired A-type stars. The plot shows the normalized frequencies of Jupiter eccentricities from observations (in orange) and from our simulations (in blue) during the post-main-sequence phase. Note that the high peak between eccentricities of 0 and 0.1 in the post-MS distribution continues beyond the frame; as we assumed very small eccentricities for all Jupiters at the beginning of our simulations, this is probably an artifact of our initial conditions. Furthermore, our simulations predict a more uniform distribution of eccentricities that continues toward higher values than currently observed. However, these higher eccentricity planets exist mostly beyond periods of ∼1000 days, making them very difficult to observe with current methods (see Figure 1, top right frame). Note that the currently highest eccentricity Jupiter observed around a "retired" A-type star does indeed have an orbital period of about 2000 days (Sato et al. 2013).

shown in Figure 1, top panels, both the MS phase as well as the post-MS phase are in agreement with the observed giant planet eccentricities (the latter depicted as black stars). We predict that there is a large population of highly eccentric planets around main sequence and retired A-type stars, as shown in Figure 5 by the blue histogram; however, most of these high-eccentricity planets have orbits longer than ∼1000 days (see Figure 1, top panels), making them difficult to observe with current methods. Interestingly, the highest eccentricity Jupiter-sized planet observed that orbits a retired A-type star, HD 120084, is very consistent with these predictions, having an eccentricity of 0.66 and a period of 2082 days (Sato et al. 2013).

Our results also indicate that most THJs will migrate to close-in orbits and get engulfed by their expanding host stars before the orbits can fully circularize, as seen in Figure 1. These planets will still have some residual eccentricities up until engulfment, consistent with a recent study of close-in planets around evolved stars (Grunblatt et al. 2018).

In our simulations, we assume that all giant planets start with very small eccentricities and treat them as singular planets around their host stars. This ignores the potential for planet–planet scattering during the further evolution. In the normalized histograms in Figure 5, we see that this artifact of our initial conditions produces an extremely high peak at small eccentricities for our simulated systems during the post-main-sequence phase (see blue histogram). This peak simply represents those systems that lie outside the parameter space that can undergo EKL oscillations. We propose that the actual initial eccentricity distribution should be more broad, probably caused by planet–planet interactions after dissipation of the planet-forming disk.

4.4. Effects of Post-MS Roche-lobe Crossing and Engulfment of THJs

A giant planet entering an expanding post-main-sequence star's Roche lobe, and subsequently the stellar envelope, can undergo and cause a multitude of effects. If the giant planet is massive and dense enough, it might resist dissipation and begin to accrete stellar material, potentially becoming a "stellar" companion undergoing complex common-envelope evolution with the main star (e.g., Soker et al. 1984). Planet engulfment should also lead to the deposition of angular momentum into the star, changing the spin rate (see Carlberg et al. 2009), which has similar consequences during the main-sequence phase (Carlberg et al. 2009; Qureshi et al. 2018), as well as the deposition of energy into the stellar envelope due to drag forces and orbital decay, increasing the luminosity of the star or producing bright UV and X-ray transients (e.g., Metzger et al. 2012; MacLeod et al. 2018). The strength of drag forces depends especially on the density of the stellar envelope and the orbital speed of the engulfed planet, which would lead to different strengths of this effect between main-sequence and post-main-sequence stars or between eccentric and circular planetary orbits. Furthermore, giant planets can have a range of masses beyond the simple Jupiter-analogs we have considered here, and can vary in density, especially if the planets are inflated due to increased temperatures (Lopez & Fortney 2016). This would lead to further variations in the possible merger outcomes (e.g., Metzger et al. 2012; Siverd et al. 2012), while also producing lithium enrichment through the engulfed giant planets of varying strengths (e.g., Aguilera-Gómez et al. 2016). The engulfment process could also lead to the ejection of material from the stellar envelope or planet, leading to the formation of dust around the star. A potential candidate for this scenario is the first-ascent giant star TYC 4144 329 2, which also has a wide separation binary companion consistent with our model (Melis et al. 2009). Overall, our predicted THJs should have a, potentially significant, influence on the evolution of their host stars post-engulfment, which could present another observable signature of THJs through increased spin rates, larger stellar luminosities, dust formation, and lithium enrichment. The effects on the further stellar evolution should also be more long-lived than the predicted few 100,000 years of existence as THJs, making indirect detection of THJs more promising than direct detection.

4.5. Occurrence Rate of HJs and THJs

To gain a better understanding of the importance of HJs and THJs as part of the overall planet population, we can estimate the fraction of systems that will produce HJs or THJs in the following way:

$$f_{\text{outcome}} = f_b f_p f_{\text{event}}, \qquad (4)$$

where f_b is the fraction of stars in binary systems, close to 100% for A-type stars (e.g., Raghavan et al. 2010; Moe & Di Stefano 2017), f_p is the fraction of Jupiter-mass planets formed at distances of a few astronomical units from their stars, which is highly uncertain, and which we extrapolate here to be $f_p \sim 0.07$–0.1 from values for G-type stars (e.g., Wright et al. 2012; Bowler 2016). Lastly, f_{event} is the fraction of simulated systems that has undergone one of the possible events specified in Table 1. For example, the percentage of systems that form HJs (during the main sequence) of all A-type

stars is $f_{HJ} \sim 0.15\%$ ($\sim 10\%$ of stars have a Jupiter, and $\sim 1.5\%$ of Jupiters become HJs), while the percentage for THJs is $f_{THJ} \sim 3.7\%$. Interestingly, $\sim 2.5\%$ of all A-type star systems will consume a Jupiter during their main-sequence lifetime and about $\sim 4.5\%$ during their post-main-sequence evolution.

We estimate the number of stars in the galaxy as $N_\star \sim (100-400) \times 10^9$, of which about 1% are in the mass range we consider here (e.g., Salpeter 1955). Thus, we can also estimate the rate at which a post-main-sequence Roche-limit crossing will take place in the galaxy (and might result in a luminosity or spin rate signature). To first order, considering the average lifetime of an A-type star to be on the order of 1 Gyr and assuming roughly uniform formation and death rates, the post-MS Roche-limit crossing rate is approximately 0.045–0.18 per year. We predict that most of these events will be caused by THJ formation and engulfment and that, given that THJs go through their orbital decay phase on the order of a few 100,000 years, there will be a few to tens of thousands of THJs in the galaxy at any given moment. The length and strength of the increased luminosity signal in red-giant stars caused by THJ engulfment and orbital energy deposition is difficult to estimate, but if it is comparable to the Kelvin–Helmholtz timescale, which is on the order of a few 10,000 years for red giants, there should be thousands of such stars with enhanced luminosities in the galaxy at any given moment. These rates indicate that THJs and their effects on post-main-sequence stars should be observable and have a strong effect on the luminosity function of intermediate mass red-giant stars.

5. Discussion

In this work, we have explored the dynamical evolution of single giant planets around A-type stars in hierarchical binaries. Considering initially circular planetary orbits between 1 and 10 au, we identify four principal evolution outcomes:

1. Classical hot Jupiters (CHJs): Giant planets that undergo high-eccentricity migration to short-period orbits ($P < 10$ days) during the main-sequence lifetime of the main star, caused by an interplay of the EKL mechanism and tidal effects. These planets can typically reach temperatures of 2000–5000 K and are eventually engulfed by the star as it expands during post-main-sequence stellar evolution. About 1.5% of our giant planets in binaries lead to this result.

2. Temporary hot Jupiters (THJs): THJs form during post-main-sequence evolution, as the stars expand. These giant planets can either form like CHJs through high-eccentricity migration caused by EKL effects and tides, or their initial orbits were close enough to their stars to eventually be heated up and engulfed by their stars even with low eccentricities ($a_1 \lesssim 3$ au). These planets only exist as HJs for a few 100,000 years before Roche-lobe crossing and engulfment, but can have significant effects on the stellar envelope and can reach temperatures of 2000–3000 K before entering the stellar Roche lobe of the expanding star. About 37% of our systems lead to this outcome.

3. Roche-limit crossers: These are giant planets that undergo very strong EKL effects that are too strong to be counteracted by tidal forces, thus crossing the Roche limit or grazing the stellar surface at high eccentricities and velocities. About 23% of our giant planets experience

this result during the stellar main sequence, while a further 8% do so in the post main sequence. During the AGB-phase, the stars lose a significant part of their mass, changing the orbital parameters of some systems enough to increase EKL strength significantly. This leads to about 0.3% of our giant planets to accrete and pollute the WD remnants through high-eccentricity Roche-limit crossing.

4. Surviving Jupiters: Gas giant planets that originally had large orbital periods and never underwent strong enough EKL effects to lead to significant interactions with their host stars. This is the case for about 30% of our systems.

Overall, only 30% of the planets will survive to the WD phase without stellar interactions, while 70% will be engulfed at some point in their evolution. The engulfed planets can have significant effects on the stellar rotation rates and luminosities. The EKL mechanism greatly enhances the fraction of planets that end up being engulfed; about 80% of engulfed planets have undergone significant EKL effects. Overall, we predict a THJ engulfment rate of ~ 0.045–0.18 per year, which, depending on the length and strength of the engulfment effects onto the red-giant stars' envelopes, could translate to thousands or tens of thousands of red giants with THJ engulfment effects at any given moment in our galaxy.

From our calculation results, we also predict that there is a large population of high-eccentricity giant planets around A-type stars with orbital periods $\gtrsim 1000$ days, which is difficult to observe, but is consistent with the known high-eccentricity giant planets. Our results are also consistent with the observed large, nearly isotropic spread of spin–orbit misalignment angles, further suggesting that stellar binary dynamics are crucial for the understanding of giant planet orbits around A-type star.

Software: SSE (Hurley et al. 2000), Matplotlib (Hunter 2007).

Appendix
A-type Stars: Definitions and Evolution

Here we give a short overview of A-type stars' evolutionary phases. A-type main-sequence stars are usually defined to have masses between ~ 1.6 and $\sim 2.4\,M_\odot$ with surface temperatures between about 7000 and 10,000 K (Adelman 2004). Figure 6 shows the evolution of temperature versus luminosity and radius for three example star masses (1.6, 2.0, and $2.4\,M_\odot$), calculated using SSE (Hurley et al. 2000).

As A-type stars evolve along the main sequence, shown in red in Figure 6, they slowly expand in radius by about a factor of two, cool down by ~ 2000–3000 K, and increase in luminosity by about a factor of two as well. Note that this
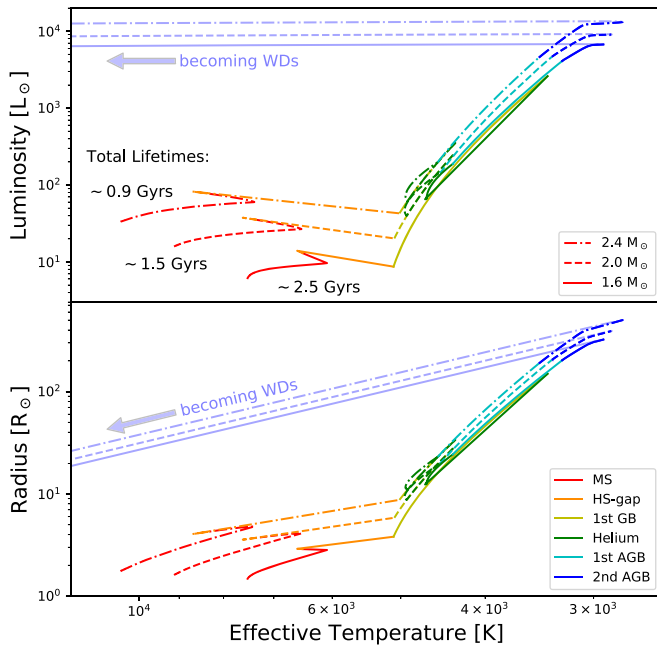
Figure 6. Stellar evolution temperature vs. luminosity and radius profiles of A-type stars. Shown are stellar evolutionary tracks for 1.6, 2.0, and 2.4 $M_\odot$ A-type stars, shown by a line, a dashed line, and a dotted–dashed line, respectively. The upper panel shows the evolution of temperature vs. luminosity, the lower panel shows temperature vs. radius. The colors of the curve segments represent different evolutionary phases, same as in Figure 1: (red) main sequence; (orange) Hertzsprung gap; (yellow) first giant branch; (green) core helium burning; (cyan) first asymptotic giant branch; (blue) second asymptotic giant branch. The light blue segment shows the evolution when the stars are becoming WDs. Lifetimes until becoming WDs for the three masses of stars are indicated in the upper panel. The lifetimes are, from low to high mass, 2.5, 1.5, and 0.9 Gyr. Tracks and times were calculated using SSE (Hurley et al. 2000).

evolution is slightly different from Sun-like G-type stars, which initially heat up during their main-sequence evolution before finally cooling down. The main-sequence phase lasts for about 2.2 Gyr for 1.6 $M_\odot$ A-type stars and 0.7 Gyr for 2.4 $M_\odot$. After they have expended their core hydrogen fuel, the stars then evolve through the Hertzsprung gap, shown in orange, rapidly expanding by another factor of two, cooling down to about 5000 K, and halving their luminosity over the course of 5–50 Myr (high to low mass).

Afterward, the first giant branch phase begins, shown in yellow, lasting for 6–100 Myr. This phase progresses very differently for low versus high mass A-type stars. A 1.6 $M_\odot$ star grows from 4 to 140 $R_\odot$, increases in luminosity from 8 to 2500 $L_\odot$ and cools down from 5000 to 3500 K, while a 2.4 $M_\odot$ star grows only from 8 to 33 $R_\odot$, increases in luminosity from 42 to 350 $L_\odot$ and cools down from 5000 to 4500 K. At the end of the first giant branch phase, the stars contract to their previous radius, luminosity, and temperature, as they begin to burn helium in their cores, shown in green. The helium burning phase lasts for about 200 Myr for 1.6 $M_\odot$ stars, 300 Myr for 2.0 $M_\odot$ stars, and 130 Myr for 2.4 $M_\odot$ stars. After expending their helium fuel, the stars rapidly evolve to become AGB giants, shown as in cyan (first ascent) and dark blue (second ascent), expanding to sizes of about 3000–4000 $R_\odot$, cooling down to 3000 K, and increasing their luminosities to about 10,000 $L_\odot$ over the course of 5–9 Myr. The stars then expel their outer layers and lose mass, becoming WDs.

In total, 1.6 $M_\odot$ stars need 2.5 Gyr, 2.0 $M_\odot$ stars need 1.5 Gyr, and 2.4 $M_\odot$ stars need 0.9 Gyr to reach the WD phase.

ORCID iDs

Alexander P. Stephan https://orcid.org/0000-0001-8220-0548
Smadar Naoz https://orcid.org/0000-0002-9802-9279
B. Scott Gaudi https://orcid.org/0000-0003-0395-9869

References

Adelman, S. J. 2004, in IAU Symp. 224, The A-Star Puzzle, ed. J. Zverko et al. (Cambridge: Cambridge Univ. Press), 1
Aguilera-Gómez, C., Chanamé, J., Pinsonneault, M. H., & Carlberg, J. K. 2016, ApJ, 829, 127
Anderson, K. R., Storch, N. I., & Lai, D. 2016, MNRAS, 456, 3671
Armitage, P. J. 2007, ApJ, 665, 1381
Armitage, P. J., Livio, M., Lubow, S. H., & Pringle, J. E. 2002, MNRAS, 334, 248
Assef, R. J., Gaudi, B. S., & Stanek, K. Z. 2009, ApJ, 701, 1616
Barnes, J. W., van Eyken, J. C., Jackson, B. K., Ciardi, D. R., & Fortney, J. J. 2013, ApJ, 774, 53
Batygin, K., & Morbidelli, A. 2013, AJ, 145, 1
Beatty, T. G., Stevens, D. J., Collins, K. A., et al. 2017, AJ, 154, 25
Beaugé, C., & Nesvorný, D. 2012, ApJ, 751, 119
Bieryla, A., Hartman, J. D., Bakos, G. Á., et al. 2014, AJ, 147, 84
Boley, A. C., Payne, M. J., & Ford, E. B. 2012, ApJ, 754, 57
Borgniet, S., Lagrange, A.-M., Meunier, N., & Galland, F. 2017, A&A, 599, A57
Bowler, B. P. 2016, PASP, 128, 102001
Bowler, B. P., Johnson, J. A., Marcy, G. W., et al. 2010, ApJ, 709, 396
Carlberg, J. K., Majewski, S. R., & Arras, P. 2009, ApJ, 700, 832
Charpinet, S., Fontaine, G., Brassard, P., et al. 2011, Natur, 480, 496
Chatterjee, S., Ford, E. B., Matsumura, S., & Rasio, F. A. 2008, ApJ, 686, 580
Collier Cameron, A., Guenther, E., Smalley, B., et al. 2010, MNRAS, 407, 507
Collier Cameron, A., & Jardine, M. 2018, MNRAS, 476, 2542
Denham, P., Naoz, S., Hoang, B.-M., Stephan, A. P., & Farr, W. M. 2018, arXiv:1802.00447
Dosopoulou, F., Naoz, S., & Kalogera, V. 2017, ApJ, 844, 12
Duquennoy, A., & Mayor, M. 1991, A&A, 248, 485
Eggleton, P. P., Kiseleva, L. G., & Hut, P. 1998, ApJ, 499, 853
Faber, J. A., Rasio, F. A., & Willems, B. 2005, Icar, 175, 248
Fabrycky, D., & Tremaine, S. 2007, ApJ, 669, 1298
Fabrycky, D. C., Johnson, E. T., & Goodman, J. 2007, ApJ, 665, 754
Farihi, J., Barstow, M. A., Redfield, S., Dufour, P., & Hambly, N. C. 2010, MNRAS, 404, 2123
Farihi, J., Jura, M., & Zuckerman, B. 2009, ApJ, 694, 805
Frewen, S. F. N., & Hansen, B. M. S. 2016, MNRAS, 455, 1538
Gaudi, B. S., Stassun, K. G., Collins, K. A., et al. 2017, Natur, 546, 514
Gaudi, B. S., & Winn, J. N. 2007, ApJ, 655, 550
Gettel, S., Wolszczan, A., Niedzielski, A., et al. 2012, ApJ, 745, 28
Ghezzi, L., Montet, B. T., & Johnson, J. A. 2018, arXiv:1804.09082
Goldreich, P., & Schlichting, H. E. 2014, AJ, 147, 32
Grunblatt, S. K., Huber, D., Gaidos, E., et al. 2018, ApJL, 861, L5
Guillochon, J., Ramirez-Ruiz, E., & Lin, D. 2011, ApJ, 732, 74
Hartman, J. D., Bakos, G. Á, Buchhave, L. A., et al. 2015, AJ, 150, 197
Howard, A. W., Marcy, G. W., Bryson, S. T., et al. 2012, ApJS, 201, 15
Hunter, J. D. 2007, CSE, 9, 90
Hurley, J. R., Pols, O. R., & Tout, C. A. 2000, MNRAS, 315, 543
Hut, P. 1980, A&A, 92, 167
Johnson, J. A., Bowler, B. P., Howard, A. W., et al. 2010a, ApJL, 721, L153
Johnson, J. A., Clanton, C., Howard, A. W., et al. 2011a, ApJS, 197, 26
Johnson, J. A., Fischer, D. A., Marcy, G. W., et al. 2007, ApJ, 665, 785
Johnson, J. A., Howard, A. W., Bowler, B. P., et al. 2010b, PASP, 122, 701
Johnson, J. A., Marcy, G. W., Fischer, D. A., et al. 2008, ApJ, 675, 784
Johnson, J. A., Morton, T. D., & Wright, J. T. 2013, ApJ, 763, 53
Johnson, J. A., Payne, M., Howard, A. W., et al. 2011b, AJ, 141, 16
Johnson, M. C., Cochran, W. D., Albrecht, S., et al. 2014, ApJ, 790, 30
Johnson, M. C., Rodriguez, J. E., Zhou, G., et al. 2018, AJ, 155, 100
Kaib, N. A., Raymond, S. N., & Duncan, M. 2013, Natur, 493, 381
Kiseleva, L. G., Eggleton, P. P., & Mikkola, S. 1998, MNRAS, 300, 292
Klein, B., Jura, M., Koester, D., & Zuckerman, B. 2011, ApJ, 741, 64
Klein, B., Jura, M., Koester, D., Zuckerman, B., & Melis, C. 2010, ApJ, 709, 950

Knutson, H. A., Fulton, B. J., Montet, B. T., et al. 2014, ApJ, 785, 126
Kozai, Y. 1962, AJ, 67, 591
Kratter, K. M., & Perets, H. B. 2012, ApJ, 753, 91
Lidov, M. L. 1962, P&SS, 9, 719
Lillo-Box, J., Barrado, D., Moya, A., et al. 2014, A&A, 562, A109
Lithwick, Y., & Wu, Y. 2012, ApJL, 756, L11
Liu, S.-F., Guillochon, J., Lin, D. N. C., & Ramirez-Ruiz, E. 2013, ApJ, 762, 37
Livio, M., & Soker, N. 2002, ApJL, 571, L161
Lloyd, J. P. 2011, ApJL, 739, L49
Lopez, E. D., & Fortney, J. J. 2016, ApJ, 818, 4
Lund, M. B., Rodriguez, J. E., Zhou, G., et al. 2017, AJ, 154, 194
MacLeod, M., Cantiello, M., & Soares-Furtado, M. 2018, ApJL, 853, L1
Masset, F. S., & Papaloizou, J. C. B. 2003, ApJ, 588, 494
Melis, C., Farihi, J., Dufour, P., et al. 2011, ApJ, 732, 90
Melis, C., Zuckerman, B., Song, I., et al. 2009, ApJ, 696, 1964
Méndez, A., & Rivera-Valentín, E. G. 2017, ApJL, 837, L1
Metzger, B. D., Giannios, D., & Spiegel, D. S. 2012, MNRAS, 425, 2778
Michaely, E., & Perets, H. B. 2014, arXiv:1406.3035
Moe, M., & Di Stefano, R. 2017, ApJS, 230, 15
Murphy, S. J., Moe, M., Kurtz, D. W., et al. 2018, MNRAS, 474, 4322
Murray-Clay, R. A., Chiang, E. I., & Murray, N. 2009, ApJ, 693, 23
Nagasawa, M., Ida, S., & Bessho, T. 2008, ApJ, 678, 498
Naoz, S. 2016, ARA&A, 54, 441
Naoz, S., Farr, W. M., Lithwick, Y., Rasio, F. A., & Teyssandier, J. 2011, Natur, 473, 187
Naoz, S., Farr, W. M., Lithwick, Y., Rasio, F. A., & Teyssandier, J. 2013a, MNRAS, 431, 2155
Naoz, S., Farr, W. M., & Rasio, F. A. 2012, ApJL, 754, L36
Naoz, S., Fragos, T., Geller, A., Stephan, A. P., & Rasio, F. A. 2016, ApJL, 822, L24
Naoz, S., Kocsis, B., Loeb, A., & Yunes, N. 2013b, ApJ, 773, 187
Ngo, H., Knutson, H. A., Hinkley, S., et al. 2016, ApJ, 827, 8
Niedzielski, A., Villaver, E., Nowak, G., et al. 2016, A&A, 589, L1
Niedzielski, A., Wolszczan, A., Nowak, G., et al. 2015, ApJ, 803, 1
North, T. S. H., Campante, T. L., Miglio, A., et al. 2017, MNRAS, 472, 1866
Nowak, G., Niedzielski, A., Wolszczan, A., Adamów, M., & Maciejewski, G. 2013, ApJ, 770, 53
Petrovich, C. 2015, ApJ, 799, 27
Petrovich, C., Malhotra, R., & Tremaine, S. 2013, ApJ, 770, 24
Qureshi, A., Naoz, S., & Shkolnik, E. 2018, arXiv:1802.08260
Raghavan, D., McAlister, H. A., Henry, T. J., et al. 2010, ApJS, 190, 1
Rasio, F. A., & Ford, E. B. 1996, Sci, 274, 954
Reffert, S., Bergmann, C., Quirrenbach, A., Trifonov, T., & Künstler, A. 2015, A&A, 574, A116
Salpeter, E. E. 1955, ApJ, 121, 161
Sato, B., Izumiura, H., Toyota, E., et al. 2008, PASJ, 60, 539
Sato, B., Omiya, M., Harakawa, H., et al. 2013, PASJ, 65, 85
Schlaufman, K. C., & Winn, J. N. 2013, ApJ, 772, 143
Shappee, B. J., & Thompson, T. A. 2013, ApJ, 766, 64
Siverd, R. J., Beatty, T. G., Pepper, J., et al. 2012, ApJ, 761, 123
Siverd, R. J., Collins, K. A., Zhou, G., et al. 2018, AJ, 155, 35
Soker, N. 1998, AJ, 116, 1308
Soker, N., & Harpaz, A. 2000, MNRAS, 317, 861
Soker, N., Livio, M., & Harpaz, A. 1984, MNRAS, 210, 189
Spiegel, D. S., & Madhusudhan, N. 2012, ApJ, 756, 132
Stello, D., Huber, D., Grundahl, F., et al. 2017, MNRAS, 472, 4110
Stephan, A. P., Naoz, S., Ghez, A. M., et al. 2016, MNRAS, 460, 3494
Stephan, A. P., Naoz, S., & Zuckerman, B. 2017, ApJL, 844, L16
Talens, G. J. J., Justesen, A. B., Albrecht, S., et al. 2018, A&A, 612, A57
Toonen, S., Hamers, A., & Portegies Zwart, S. 2016, ComAC, 3, 6
van Lieshout, R., Kral, Q., Charnoz, S., Wyatt, M. C., & Shannon, A. 2018, arXiv:1805.04429
van Saders, J. L., & Pinsonneault, M. H. 2013, ApJ, 776, 67
Villaver, E., & Livio, M. 2009, ApJL, 705, L81
Wittenmyer, R. A., Gao, D., Hu, S. M., et al. 2015a, PASP, 127, 1021
Wittenmyer, R. A., Horner, J., Tinney, C. G., et al. 2014, ApJ, 783, 103
Wittenmyer, R. A., Wang, L., Liu, F., et al. 2015b, ApJ, 800, 74
Wright, J. T., Marcy, G. W., Howard, A. W., et al. 2012, ApJ, 753, 160
Wu, Y., & Lithwick, Y. 2011, ApJ, 735, 109
Wu, Y., Murray, N. W., & Ramsahai, J. M. 2007, ApJ, 670, 820
Xu, S., Jura, M., Klein, B., Koester, D., & Zuckerman, B. 2013, ApJ, 766, 132
Xu, S., Zuckerman, B., Dufour, P., et al. 2017, ApJL, 836, L7
Zahn, J.-P. 1977, A&A, 57, 383
Zhou, G., Rodriguez, J. E., Collins, K. A., et al. 2016, AJ, 152, 136
Zuckerman, B., Koester, D., Dufour, P., et al. 2011, ApJ, 739, 101